Gain-Assisted Propagation in a Plasmonic Waveguide at Telecom Wavelength

Jonathan Grandidier, Gérard Colas des Francs,* Sébastien Massenot, Alexandre Bouhelier, Laurent Markey, Jean-Claude Weeber, Christophe Finot, and Alain Dereux

Institut Carnot de Bourgogne, UMR 5209 CNRS et Université de Bourgogne, 9, avenue A. Savary, BP 47870, 21 078 Dijon, France

ABSTRACT

The spatial confinement of surface plasmon polaritons is a promising route for realizing optical on-board interconnects. However, mode losses increase with the confinement factor. To overcome this road block, we investigate propagation assisted by stimulated emission in a polymer strip-loaded plasmonic waveguide doped with nanocrystals. We achieve 27% increase of the propagation length at telecom wavelength corresponding to a 160 cm^{-1} optical gain coefficient. Such a configuration is a step toward integrated plasmonic amplifiers.

At the interface between molecular optics and solid state physics, molecular plasmonics combines chemical engineering and surface plasmon polaritons (SPPs) properties to produce hybrid materials available for biosensing, data storage, photovoltaic cells, or integrated photonic applications.[1] In particular, the design of a surface plasmon circuitry is the object of intense research due to its ability to transfer optical information on a subwavelength scale. In the last years, a large set of passive plasmonic components were integrated to control and manipulate SPPs in a planar circuitry.[2] Very recently, the feasibility of using SPP waveguides for achieving 10 Gbit/s chip-to-chip data transfer has been demonstrated.[3] Recent works also proposed novel configurations to realize all-optical active SPP functionalities[4−7] or to utilize quantum effects related with SPPs.[8] These approaches are however plagued by the existing trade-off between confinement and propagation. To overcome this stringent limitation, strategies are emerging to reduce the intrinsic losses associated to SPP modes existing on metal surfaces. In particular, stimulated emission of surface plasmons exploiting optical pumping of molecular dyes[9,10] or erbium ions[11] was recently demonstrated for weakly confined modes. In this letter, we demonstrate an increase of propagation length for confined SPP modes in dielectric-loaded surface plasmon polariton waveguides (DLSPPWs). A DLSPPW typically consists of a dielectric strip - usually a polymer - deposited on a metal film.[12] Efficient integration of passive components based on this technology was recently demonstrated.[13,14] These waveguid-

ing structures are characterized by a large confinement factor of the mode inside the polymer structure at the expense of a reduced propagation length.[15] To address this shortcoming, we developed a strategy to partially compensate confinement-induced SPP losses by doping the DLSPPW polymer layer with quantum dots (QDs) nanocrystals undergoing stimulated emission. We therefore take advantage of an efficient overlap between the SPP mode and the active material.

Lead sulfide (PbS) QDs (Evident Technologies, concentration in the waveguide $N \sim 9 \times 10^{16}$ cm^{-3}) were inserted in a polymethylmethacrylate (PMMA) polymer strip waveguide fabricated on a 40 ± 3 nm thick gold film using a UV-lithography technique (Figure 1, and Supporting Information). These QDs were chosen for their high photostability and tunability.[16] The waveguide thickness and width were adjusted for single mode operation. This waveguide geometry supports a TM (transverse magnetic)-polarized SPP mode propagating along the guide axis. The magnetic field writes

$$\mathbf{H}(x, y, z) = H_0(x,z)\exp(i(k_{\text{spp}}y - \omega t)\exp(-y/2L_{\text{spp}})\boldsymbol{e_x}$$

(1)

where k_{SPP} and L_{SPP} are the wave-vector and attenuation length of the mode, respectively. Experimentally, k_{SPP} and L_{SPP} are evaluated from leakage radiation microscopy images recorded in the Fourier and images planes[15] (Supporting Information). In the image plane, the detected intensity is

$$I(x, y) \propto |\mathbf{H}(x, y, z_0)|^2 = |H_0(x, z_0)|^2\exp(-y/L_{\text{spp}})$$
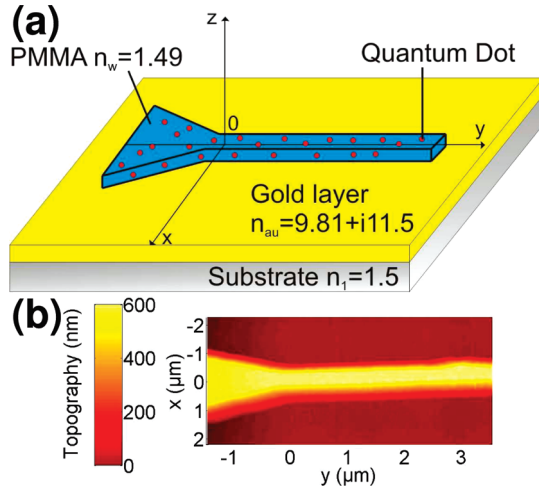
(2)

Figure 1. (a) DLSPPW configuration. A PMMA strip confines the plasmon at the gold/polymer interface. An additional tapering structure is designed to efficiently excite the SPP guided mode with an external infrared laser (Figure 3a). The effectives indices used in the numerical simulations are indicated on the figure. (b) Atomic force microscopy image of the DLSPPW. The dimensions of the waveguide are 600 nm height, 400 nm width, and 65 μm long.

where z_0 is the objective focal point. Hence, the propagation length L_{SPP} can be readily inferred by measuring the SPP intensity distribution. In the Fourier plane, the recorded signal is

$$I(k_x, k_y) \propto |\tilde{H}(k_x, k_y, z_0)|^2 = \frac{|\tilde{H}_0(k_x, z_0)|^2}{(k_y - k_{SPP})^2 + (1/2L_{SPP})^2} \quad (3)$$

where tilde stands for Fourier transform. The intensity recorded in the Fourier plane has a Lorentzian shape centered on the wave-vector of the mode k_{SPP} and with a full-width-at-half-maximum (FWHM) given by $1/L_{SPP}$.

We first investigated the coupling of QDs emission into waveguide modes (Figure 2). A 532 nm laser was focused on the doped polymer waveguide to pump the QDs in their excited states. The fluorescence emitted around 1500 nm was recorded in the image plane (Figure 2a). A vertical trace extending on either sides of the excitation area indicates a guided mode. Figure 2b shows the modal distribution of effective indices measured in the Fourier plane. The image was obtained for a large excitation area in order to identify all the modes supported by the fabricated structures (see also the inset of Figure 2c). One horizontal line labeled TM_{00} is visible at an effective index $n_{eff} = k_y/k_0 = 1.18$ (k_0 is the free space wavenumber).[15] This is the signature of a mode propagating inside the DLSPPW with a constant k_y wave-vector. Importantly for the following, this mode results from the preferential decay of QDs spontaneous emission into a SPP mode supported by the DLSPPW. The single mode nature of the DSLPPW is evident from Figure 2a,b. Additionally, three arcs of a circle are also visible in Figure 2b, indicating an isotropic propagation of a mode in the surface plane. The inner circle originates from fluorescence coupling to a gold/air SPP mode ($n_{eff} \sim 1.0$) located on either
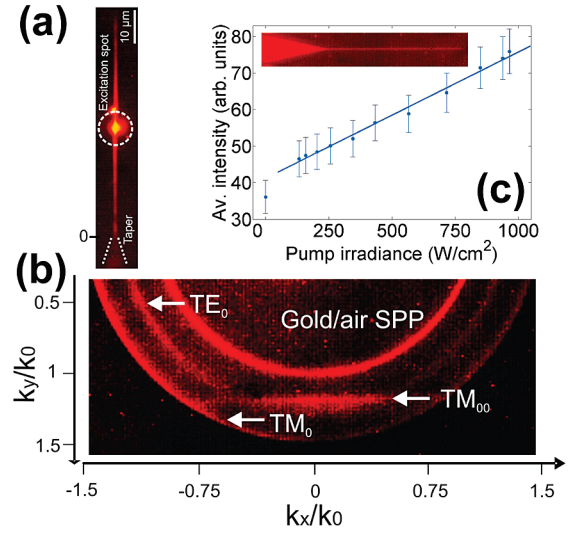

Figure 2. (a) QDs fluorescence (emission wavelength around 1.5 μm) recorded in the image plane. The QDs are excited with a laser ($\lambda = 532$ nm, NA = 0.16) focused at the center of the guide (bright spot). Two fluorescence traces extending on both sides of the excitation spot indicates that the emission is coupled to guided modes. (b) QDs fluorescence recorded in the Fourier plane for an extended defocused excitation. The arrows indicate the different effective indices ($n_{eff} = k_y/k_0$) of the modes existing within the illuminated area. The gold/air SPP mode effective index ($n_{eff} \sim 1$) and objective numerical aperture (NA = 1.49) were used to calibrate the Fourier plane. The image is saturated for clarity. (c) Averaged spontaneous emission intensity for increasing pump powers (dots, standard deviation indicated) with a linear regression (blue line). The inset shows an homogeneous emission inside the waveguide since an extended illumination was used.

side of the DLSPPW. The two other circles are assigned to film modes existing inside the PMMA tapering region adjacent to the waveguide (Figure 1). Specifically, they are a TM_0 gold/PMMA surface plasmon ($n_{eff} \sim 1.46$) and a transverse electric TE_0 mode ($n_{eff} \sim 1.22$) guided into the large tapered PMMA portion. Both TM and TE modes are excited due to the unpolarized emission of the QDs and the multimodal character of the 600 nm thick polymer taper. Using the Differential method,[17] we calculated the effective indices of the detected modes. We obtained $n_{eff}(TM_{00}) = 1.18$, $n_{eff}(TM_0) = 1.45$, and $n_{eff}(TE_0) = 1.20$ at $\lambda = 1.525$ μm (QDs emission peak) in agreement with the measured values. Finally, Figure 2c shows the QDs spontaneous emission intensity versus pump power. The emission intensity was measured as being the intensity averaged over the complete waveguide homogeneously excited. As expected from spontaneous decay, this signal linearly increases with pump power.

The doped PMMA layer can act as a gain medium for the DLSPPW guided mode if the QDs can undergo stimulated emission into SPPs.[11] To this aim, a TM-polarized infrared laser beam ($\lambda = 1.55$ μm) is focused on the tapering region to excite a SPP mode.[18] Figure 3a shows the single-exponential decay of the laser-coupled mode along the waveguide ($L_{SPP} = 13.6 \pm 0.8$ μm) and its intensity distribution (inset) without pumping the QDs. Because of QDs absorption, L_{SPP} is slightly lower than the propagation length measured in an undoped (passive) waveguide (L_{SPP}
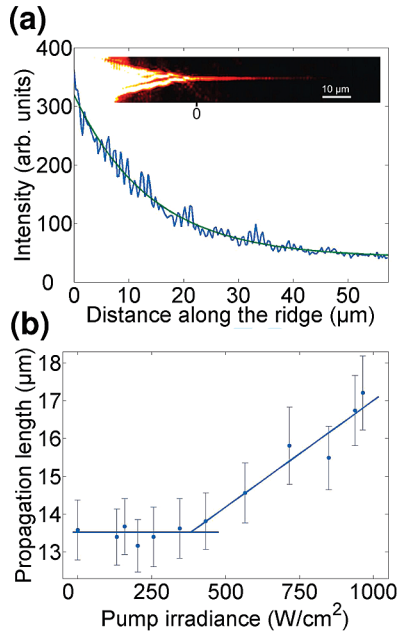
Figure 3. (a) Attenuation length of the SPP mode inside the DLSPPW measured in absence of QDs pumping (blue curve). The data can be fitted by a single exponential decay of the form of eq 2 (green curve) with a decay constant of 13.6 μm. Inset: Image of the intensity distribution of the mode inside the waveguide. The SPP guided mode is excited by focusing an infrared laser beam ($\lambda = 1.55 \, \mu$m) onto the tapering region. (b) Propagation length measured for increasing pump irradiance ($\lambda = 532$ nm) at constant IR laser power (dots). The blue curve is a guide for the eyes.

$= 14.1 \pm 0.5 \, \mu$m) with the same dimensions. We note that this difference is small due to the low concentration of QDs within the waveguide ($N \sim 9 \times 10^{16}$ cm^{-3} corresponding to a volume fraction $f = 7$ per thousand). This low propagation length originates from strong radiative losses. This allows rapid investigation by leakage radiation microscopy, limiting thus QDs photobleaching.

To investigate the influence of the pumped QDs on the SPP guided mode, the waveguide is homogeneously excited by the 532 nm pump beam (see Figure S2 of Supporting Information). Figure 3b presents the fitted propagation lengths L_{SPP} (I_P) as a function of pump irradiance I_P. The propagation length remains constant around 13.5 μm for pump irradiance below 500 W·cm^{-2} and increases up to 17.2 $\pm$ 1 μm for 1000 W·cm^{-2}, exceeding the propagation length of the undoped waveguide. This 27% net gain cannot be solely explained by a thermal variation of the optical index of the PMMA,[4] suggesting a contribution of stimulated emission of SPPs.[9−11] A signature of stimulated emission is a spectral narrowing of the emitted light.[10] To check this, we used a single-mode fiber-coupled spectrograph working at room temperature. Unfortunately, the combination of coupling losses, weak signal-to-noise ratio at ambient temperature and limited acquisition time (photobleaching) prevented an unambiguous demonstration of a spectral narrowing.

Nevertheless, stimulated emission was qualitatively confirmed by a line width narrowing of the effective index of the DLSPPW mode. Stimulated emission of SPP can be
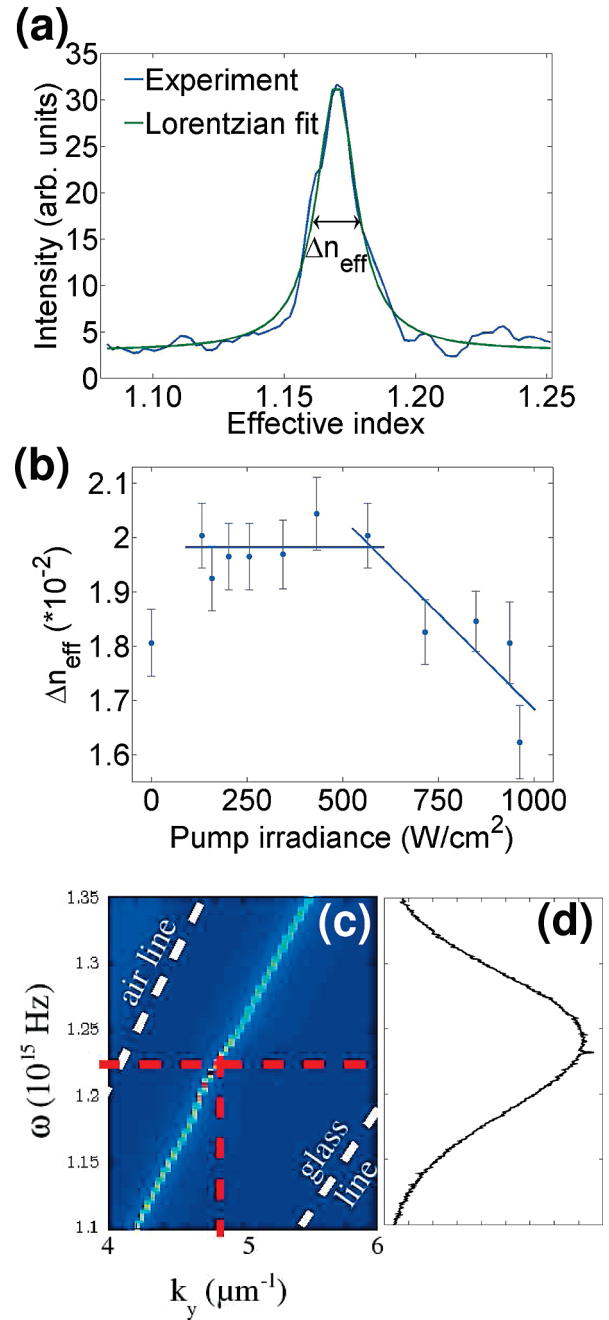

Figure 4. (a) Effective index line width of the DLSPPW mode measured in the Fourier plane without QDs excitation (blue curve). The line width is well approximated by a Lorentzian fit (green curve, see also eq 3). (b) Full-width-half-maximum (FWHM) of the effective index variation Δn_{eff} versus pump irradiance. (c) Density of mode calculated as a function of wave vector k_y and free space frequency ω. Red dotted lines correspond to $\lambda = 1.55 \, \mu$m excitation. (d) QDs emission spectrum. Comparing panels c and d, we see that the mode wave-vector varies from $k_y = 4.5 \, \mu$m^{-1} ($n_{eff} = 1.17$) to $k_y = 5.4 \, \mu$m^{-1} ($n_{eff} = 1.24$) on QDs emission spectrum FWHM.

either investigated in frequency space at a fixed mode momentum or in momentum space at a fixed frequency (see, e.g., Figure 2 of ref 10). On the basis of a Fourier analysis of the mode propagation, we report in Figure 4 the effect of stimulated emission on the effective index line width. The stimulated emission is associated with a narrowing of the coupled wave-vectors because the resulting mode is strictly
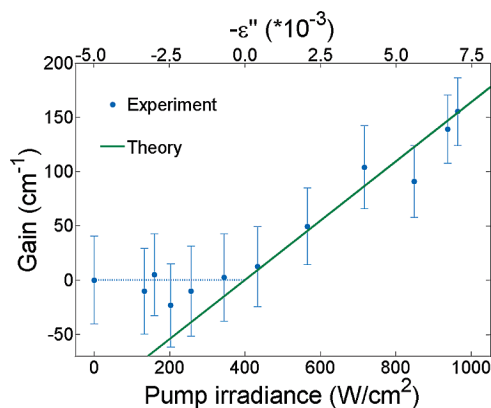
Figure 5. Intrinsic optical gain coefficient $g = [1/L_{SPP}(0) - 1/L_{SPP}(I_p)]$ measured versus pump irradiance (blue dots, bottom scale) or calculated as a function of the imaginary part ε'' of the DLSPPW dielectric constant (green line, top scale).

identical to the SPP mode responsible for the stimulation. Below the transparency threshold (population inversion), the mode width is mainly governed by the large QDs emission spectrum so that the effective index width remains approximately constant for pump powers below 500 W·cm^{-2} (Figure 4b). More precisely, Figure 4c represents the density of modes calculated in the QDs emission spectrum range, revealing the dispersion relation $\omega = f(k_y)$.[19] For low pumping power, the QDs spontaneous emission couples to the DLSPPW mode with a large spectrum, leading to an effective index broadening (see also Supporting Information). When the population inversion is achieved, stimulated emission increases the amount of energy coupled into the mode propagating at $\lambda = 1.55\ \mu$m. Figure 4b clearly shows a decrease of the effective index line width above 500 W·cm^{-2}. This line width narrowing indicates that stimulated emission of SPP[10,11] occurs in conjunction with a net increase of L_{spp} (Figure 3b). Importantly, the observed narrowing of the effective index comes from two contributions, which are not independent. The first contribution originates from a compensation of the losses. Reducing the losses strongly narrows the mode line width since $\Delta k_{//}(\lambda) = 1/L_{SPP}(\lambda)$. The second contribution is the result of a decrease in the contribution of the spontaneous decay channel in favor of the stimulated emission channel.

Finally, the optical gain coefficient $g = [1/L_{SPP}(0) - 1/L_{SPP}(I_P)]$ is reported versus pump irradiance in Figure 5. g was compared to numerical simulations obtained by imposing negative values to the imaginary part ε'' of the waveguide dielectric constant. The gold layer thickness was adjusted to 35 nm so that the propagation length calculated for $\varepsilon'' = 0$ equalizes the one measured without pump. The small difference with the experimental thickness (40 nm) is explained by additional extrinsic radiative losses due to scattering by gold roughness and PbS nanocrystals. ε'' can be estimated[10] from the QDs density ($N \sim 9 \times 10^{16}$ cm^{-3}), their emission rate ($\gamma \sim 10^6$ s^{-1}), their absorption ($\sigma_a = 4.3 \times 10^{-15}$ cm^2), and their stimulated emission (σ_{st}) cross sections. σ_{st} is an unknown parameter and was adjusted at 3×10^{-15} cm^2 to reproduce the experimental gain at 1000 W·cm^{-2}. This value is probably underestimated due to

emission quenching near the metal so that more refined models should be considered.[20] Nonetheless, the experimental optical gain is qualitatively well reproduced by the theoretical curve above the transparency threshold ($\sim$500 W·cm^{-2}).

In conclusion, our experimental results unambiguously demonstrate the occurrence of a surface plasmon polariton optical gain by stimulated emission of SPPs in a waveguiding architecture. The gain obtained partially compensates the losses introduced by confining a plasmon. While this does not constitute an amplification, several strategies are possible to realize a plasmonic amplifier. Optical gain in PbS quantum dots is limited due to the 8-fold degeneracy of the first excited states requiring at least four excitons for population inversion.[21] An optimized gain medium as well as thicker gold films (reduced SPP radiative losses) would certainly contribute to enhance the optical gain. Finally, different strategies for active pumping can also be investigated such as semiconductor electrical pumping.[22,23] The realization of integrated plasmonics amplifiers could represent a key step toward miniaturized all-optical on-board interconnects.

Supporting Information Available: Doped waveguide fabrication, leakage radiation microscopy setup, and detailed discussion of effective index broadening. This material is available free of charge via the Internet at http://pubs.acs.org.

References
(1) Van Duyne, P. *Science* **2004**, *306*, 985–986.
(2) Ebbesen, T.; Genet, C.; Bozhevolnyi, S. *Phys. Today* **2008**, *61*, 44–50.
(3) Kim, J. T.; Ju, J. J.; Park, S.; Kim, M.; Park, S. K.; Lee, M. H. *Opt. Express* **2008**, *16*, 13133–13138.
(4) Lereu, A. L.; Passian, A.; Goudonnet, J.-P.; Thundat, T.; Ferrell, T. L. *Appl. Phys. Lett.* **2005**, *86*, 154101.
(5) Dintinger, J.; Klein, S.; Ebbesen, T. *Adv. Mater.* **2006**, *18*, 1267–1270.
(6) Wiederrecht, G. P.; Hall, J. E.; Bouhelier, A. *Phys. Rev. Lett.* **2007**, *98*, 83801.
(7) Pacifici, D.; Lezec, H. J.; Atwater, H. A. *Nat. Photonics* **2007**, *1*, 402–406.
(8) Bergman, D.; Stockman, M. *Phys. Rev. Lett.* **2003**, *90*, 27402.
(9) Seidel, J.; Grafström, S.; Eng, L. *Phys. Rev. Lett.* **2005**, *94*, 177401.
(10) Noginov, M. A.; Zhu, G.; Mayy, M.; Ritzo, B. A.; Nogovina, N.; Podolskiy, V. A. *Phys. Rev. Lett.* **2008**, *101*, 226806.
(11) Ambati, M.; Nam, S. H.; Ulin-Avila, E.; Genov, A.; Bartal, G.; Zhang, X. *Nano Lett.* **2008**, *8*, 3998–4001.
(12) Hohenau, A.; Krenn, J. K.; Stepanov, A. L.; Drezet, A.; Ditlbacher, H.; Steinberger, B.; Leitner, A.; Ausseneg, F. R. *Opt. Lett.* **2005**, *30*, 893–895.
(13) Krasavin, A. V.; Zayats, A. *Phys. Rev. B* **2008**, *78*, 45425.
(14) Holmgaard, T.; Chen, Z.; Bozhevolnyi, S. I.; Markey, L.; Dereux, A.; Krasavin, A. V.; Zayats, A. V. *Appl. Phys. Lett.* **2009**, *94*, 51111.
(15) Grandidier, J.; Massenot, S.; Colas des Francs, G.; Bouhelier, A.; Weeber, J. C.; Markey, L.; Dereux, A.; Renger, J.; Gonzalez, M. U.; Quidant, R. *Phys. Rev. B* **2008**, *78*, 245419.
(16) Klimov, V. I.; Mikhailovsky, A. A.; Xu, S.; Malko, A.; Holligsworth, J. A.; Leatherdale, C. A.; Eisler, H. J.; Bawendi, M. G. *Science* **2000**, *290*, 314–316.

(17) Massenot, S.; Weeber, J. C.; Bouhelier, A.; Colas des Francs, G.; Grandidier, J.; Markey, L.; Dereux, A. *Opt. Express* **2008**, *16*, 17599–17608.

(18) Holmgaard, T.; Bozhelvolnyi, S.; Markey, L.; Dereux, A. *Appl. Phys. Lett.* **2008**, *92*, 11124.

(19) Manjacas, A.; Garcia de Abajo, F. J. *Nano Lett.* **2009**, *9*, 1285–1289.

(20) De Leon, I.; Berini, P. *Phys. Rev. B* **2008**, *78*, 161401(R).

(21) Hoogland, S.; Sukhovatkin, V.; Howard, I.; Cauchi, S.; Levina, L.; Sargent, E. H. *Opt. Express* **2006**, *14*, 3273–3281.

(22) Sirtori, C.; Gmachl, C.; Capasso, F.; Faid, J.; Sivco, D. L.; Hutchinson, A. L.; Cho, A. Y. *Opt. Lett.* **1998**, *23*, 1366–1368.

(23) Kumar, P.; Tripathi, V. K.; Liu, C. S. *J. Appl. Phys.* **2008**, *104*, 33306.

NL901314U